frontiers | Frontiers in Energy Research

TYPE Original Research
PUBLISHED 11 November 2024
DOI 10.3389/fenrg.2024.1406457

OPEN ACCESS

EDITED BY
Feng Dong,
China University of Geosciences, China

REVIEWED BY
Jingya Zhang,
Research Institute of Petroleum Exploration and Development (RIPED), China
Cunqi Jia,
The University of Texas at Austin, United States
Jiazheng Qin,
Southwest Petroleum University, China

*CORRESPONDENCE
Zhang Hui,
zhanghui01_cq@petrochina.com.cn

RECEIVED 25 March 2024
ACCEPTED 14 August 2024
PUBLISHED 11 November 2024

CITATION
Yunhe S, Hui Z, Bo P, Xueyuan J, Xiaowei D and Xiaohu Z (2024) Three-dimensional spatial structure and heterogeneity characterization of #5 coal of Shanxi Formation in eastern Ordos basin.
Front. Energy Res. 12:1406457.
doi: 10.3389/fenrg.2024.1406457

Three-dimensional spatial structure and heterogeneity characterization of #5 coal of Shanxi Formation in eastern Ordos basin

Shi Yunhe[1], Zhang Hui[1]*, Pan Bo[1], Jing Xueyuan[1], Du Xiaowei[1] and Zhou Xiaohu[2]

[1]PetroChina Company Limited Changqing Oilfield Branch, Xi'an, Shaanxi, China, [2]Department of Geology/State Key Laboratory of Continental Dynamics, Northwest University, Xi'an, China

Based on macroscopic qualitative observation, microscopic quantitative analysis, low-temperature adsorption, high-pressure mercury intrusion and three-dimensional CT scanning, the spatial structure and heterogeneity of the #5 coal from the eastern Ordos Basin, Shanxi Formation, are quantitatively characterized. The following observation were studied: 1) The main body of the #5 coal was intact structural coal seam, with the density of cleats gradually increasing from north to south. 2) The microscopic composition of the #5 coal is dominated by desmocollinite, which contains small amounts of inertinite and inorganic minerals, with the inorganic component mainly composed of carbonate rocks and a small amount of clay. The carbon content and the content of its inorganic minerals in the #5 coal gradually decrease toward the inner basin, caused by transport distance and depositional environment. 3) At the micrometer scale, no significant pores were observed, and the #5 coal bed is primarily composed of micro-mesopores smaller than 40 nm, with a small number of 50~100 nm macropores. Simultaneously, micro-fractures in the coal bed were well developed; by using mercury intrusion data of the bimodal feature of the pore throat, indicates the coexistence of micrometer-scale micro-fractures and nanometer-scale mesopores within the coal, with pronounced differences and interconnected complexity. 4) The porosity and permeability of microfractures, as well as the number of microfracture bars and permeability, indicate that the connectivity of coal bed is primarily caused by the microfracture system. By reconstructing the three-dimensional spatial structure of the #5 coal through multiple tests, the heterogeneous characteristics are quantitatively characterized.

KEYWORDS

3D spatial structure, heterogeneity, #5 coal, Upper Paleozoic, eastern Ordos basin

1 Introduction

Coal bed methane (CBM) is an unconventional natural gas generated from coal seam, and its main component is methane which primarily stored in the pores of coal seam in an adsorbed state. Coal is a porous medium with a dual-porosity system, and the processes of adsorption, desorption, permeation, and diffusion of coalbed methane were significantly

contributed by the micro-pore structure of coal. Therefore, the pore system of coal reservoirs is the primary factor of the occurrence and production of coalbed methane, and affects the efficiency of coalbed methane extraction during the development and production stages (Tissot and Welte, 1984; Stach et al., 1990; Levy et al., 1997; Crosdale et al., 1998; Clarkson and Bustin, 1999; Chou, 2012; Qin and Shen, 2016; Li et al., 2017). Microscopic structural analysis of coal typically involves qualitative and quantitative analysis of coal micro-pore-fracture structures using techniques such as microscopic imaging, mercury intrusion Porosimetry, low-temperature adsorption, scanning electron microscopy, CT scanning, etc., to analyze and discuss the different characteristics in microstructural parameters of coal seams (Yao et al., 2010; Chalmer et al., 2012; Cnudde and Boone, 2013; Shan et al., 2014; Nie et al., 2015; Hou et al., 2017; Chen et al., 2020; Dai et al., 2022; Zhao et al., 2023).

Comprehensive results of previous researches concluded that the internal pore structure of coal seams can be visualized clearly and quantified by scanning electron microscopy and micrometer CT scanning. However, those tests have limitations in terms of quantifying nanoscale microporous parameter (Cnudde and Boone, 2013; Li et al., 2014; Li et al., 2016). Although mercury intrusion and low-temperature adsorption can be used to achieve the structural characteristics of micropores and mesopores in coal seams, and reconstructing pore size distribution and connectivity, all these test results cannot distinguish micropores from fractures, which are usually considered to be the similar system (Hu et al., 2003; Song et al., 2017; Jiang et al., 2010).

This study is initially evaluated the micropores, throat structure, fracture development, mineral filling conditions, and their spatial patterns. Subsequently, through the reconstruction of coal's three-dimensional images, it quantitatively characterized the three-dimensional spatial structure of coal and the heterogeneity of the reservoir. Finally, by leveraging the comprehensive analysis of various test results, it examined the intrinsic connections among the pore distributions obtained through different experimental methods, concluded multi-parameter characterization of the coal seam pore structure, and a comprehensive and intuitive understanding of the micropore-microfracture system within coal seams.

2 Materials and methods

2.1 Geologic setting and samples

The Ordos Basin is the second-largest sedimentary basin in China and constitutes a part of the North China Craton. During the Carboniferous-Permian period, the North China Craton existed as a sizable island situated near the ancient equator of the Pan-Mediterranean Sea (Torsvik and Cocks, 2004). Over the Paleozoic era, the coal-bearing basins of North China underwent a gradual transition from marine-transitional to terrestrial sedimentation (Li et al., 2019). This epoch of warm and humid climatic conditions, coupled with extensive coastal platforms, provided conducive environments for the formation of peat swamps and subsequent coal deposition. Consequently, the Upper Paleozoic coal resources within the Ordos Basin are abundant and widely distributed. Notably, both the #8 coal at the summit of the Benxi Formation in the Upper Carboniferous and the #5 coal of Shanxi Formation in the Lower Permian serve as regional marker beds. In the eastern sector of the basin, the #5 coal is relatively shallowly buried, thereby facilitating its exploitation (Figure 1).

The Upper Paleozoic gas source rocks in the Ordos Basin exhibit characteristics of "extensively-covered hydrocarbon expulsion" and "cumulative gas accumulation": Organic matter maturity in the majority of the central basin has reached the stages of thermogenic condensate-rich gas generation and dry gas generation (Liu et al., 2007; Yang et al., 2012; Cao et al., 2013). The latest gas enrichment patterns suggest a closer affinity to a "quasi-continuous accumulation model" (Zhao et al., 2013; Zhao et al., 2017). Natural gas is primarily generated from the Middle Jurassic to Early Cretaceous. The main gas-bearing intervals in the Upper Paleozoic of the basin are the lithic quartz sandstones of the He 8 Member in the western area and the quartz sandstones of the Shan 2 Member in the eastern area. The analyzation of #5 coal in this study is directly deposited on top of the Shan 2 Member of Shanxi Formation.

Although there are a large number of exploration wells in the Eastern Ordos Basin, there are not many sampling wells to choose because one-quarter the drilled wells preserved cores that were only sandstone and did not coal seams. Thick and multiple sets of coal seams were selected and sampled, which were in order to analyze not only vertical trends in single well but also planar trends about #5 coal. Samples were distributed throughout the study area as much as possible, which helps to reduce sample selection bias and brings the samples closer to the overall coal seam characteristics. Six coal samples from comparatively thick coal seams with micro-fractures that can be visualized, which were selected as primary targets for three-dimensional reconstruction testing. So 76 samples from 35 wells in the Eastern Ordos Basin were selected, which combined analysis with their maceral group composition, minerals, porosity and permeability, a multi-scale and multi-parameter joint characterization of the coal seam micro-pore and micro-fractures structure in the Upper Paleozoic was conducted accordingly (Figure 1).

2.2 Methods

Various coal tests were conducted at the State Key Laboratory of Continental Dynamics (Northwest University) by using several instruments, including a transmission light-fluorescence microscope (Leica 6M), fluorescence spectrometer, confocal microscope with white light (Leica TCS SP8), adsorption analyzer (Quantachrome Quadrasorb), micro-CT (ZEISS Xradia 520 Versa), and mercury porosimeter (Quantachrome poremaster). These tests followed the procedures and technical requirements outlined in standard methods, Include the GB/T 16773-2008 (Method of preparing coal samples for coal petrographic analysis), GB/T 12937-2008 (Terms relating to coal petrology), GB/T 8899-2013 (Determination of maceral group composition and minerals in coal), GB/T 30732-2014(Proximate analysis of coal -Instrumental method), and MT/T 507-2019 (General rules of coal petrographic analysis).

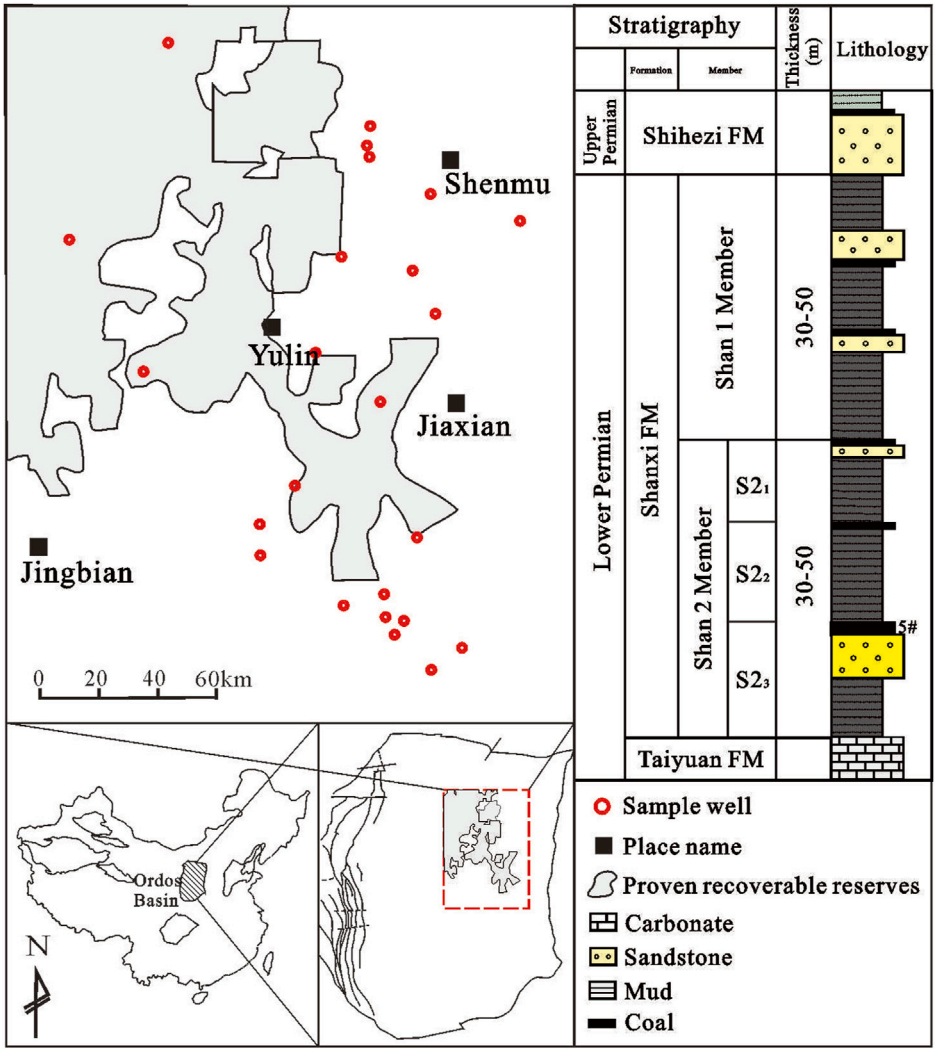

FIGURE 1
Division of tectonic units and location of the samples.

Systematic testing to quantify coal industry components at first, which can acquire the carbon content and ash value. Based on the coal component data, half of the samples were selected for XRD and microscopic composition testing, which could further quantify the mineral composition and micro macerals and minerals. On the basis of the micro-image analysis, the samples in which micro-fractures were observed have been subjected to laser confocal testing to analyze their width and trapped period.

Semi-quantitative measurements and analysis about micro-fractures from microscopic images at first. The nanopores were quantitative analyzed by low-temperature adsorption (N_2 +CO_2) because these nanopores could not be observed by microscopic images Subsequently. Then quantify the nanopores and micro-fractures by high-pressure mercury intrusion test at the same time, and establish the correlation analysis between the micrometer-scale and nanoscale test results, thereby explaining the presence of bimodal features of pore throat radius in coal by multiple tests.

3 Results and discussion

3.1 Classification of macro-composition

The macroscopic composition of the #5 coal in Shanxi Formation is predominantly semi-bright coal and bright coal, with relatively fewer semi-dark coals. Overall, there is an increasing proportion of semi-bright coal (Figures 2A–D) and bright coal (Figures 2E–I) from Shenmu to Jingbian, accompanied by a decreasing trend in semi-dark coal and dull coal. Macroscopic observations indicate that the main body of the #5 coal consists of intact coal, with a small amount of fractured coal observed in the southern Jiaxian area. Cleats are well-developed within the coal across different well locations.

A large number of high-angle fractures, typically developed perpendicular to bedding, are observed, often filled with minerals such as white calcite, forming a network of calcite-filled fractures (Figure 2, indicated by blue arrows). Statistical observations from

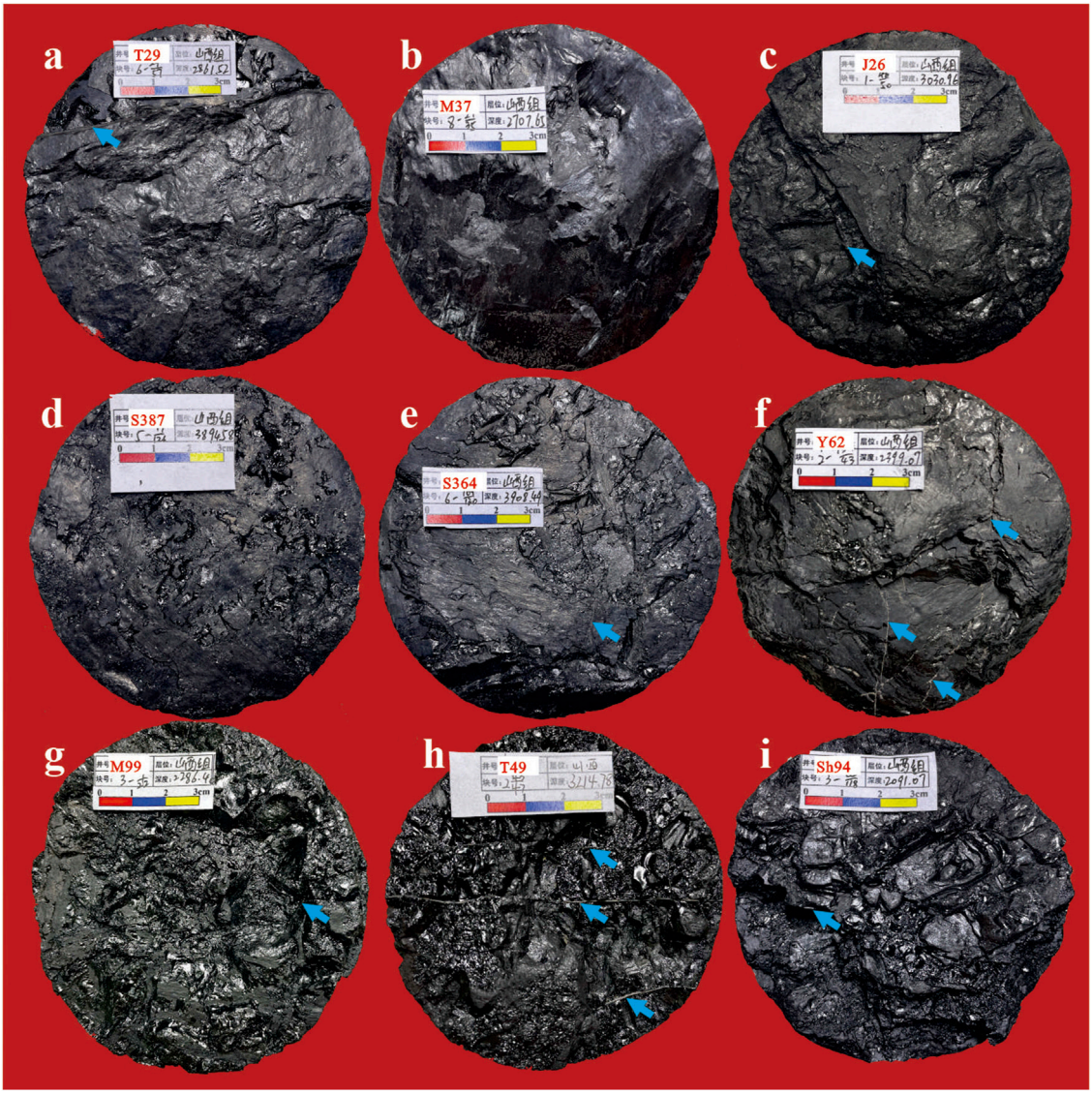

FIGURE 2
Macro-composition characteristics of #5 coal ((**A**)-T29 2861.5 m, (**B**)-M37 2707.6 m, (**C**)-J26 3030.9 m, (**D**)-S387 3494.5 m, (**E**)-S364 3908.4 m, (**F**)-Y62 2399 m; (**G**)-M99 2296.4 m, (**H**)-T49 3214.7 m, (**I**)-Sh94 2091 m).

core analysis demonstrate a gradual increase in cleat density and intensity from north to south.

3.2 Micro macerals and minerals

The microscopic composition of the #5 coal in Shanxi Formation is predominantly vitrinite, ranging from 56.6% to 93.78%, with a mean value of 75.45%. Within the vitrinite, the majority comprises desmocollinite, followed by telocollinite and telovitrinite (Figures 3A–C). The content of inertinite varies significantly, ranging from 0.02% to 31.33%, with a mean value of 11.29%, while exinite is relatively less abundant, with a mean value of 2.6%.

The content of inorganic minerals ranges from 1.33% to 23.65%, with an average value of 10.90%. The predominant inorganic component is carbonate rocks, with small amounts of clay. The inorganic minerals exhibit a banded distribution under the microscope, with some grains semi-oriented along their long axes (Figure 3C). Under blue light excitation, exhibits no significant fluorescence (Figure 3A), displays a weak tawny-yellow fluorescence, while calcite cements exhibit yellow-green fluorescence. Early non-directional fractures, resulting from hydrocarbon generation, typically show relatively wide and curved surfaces, whereas later fractures, filled with carbonate, tend to appear straight and narrower.

At the microscopic scale, no obvious pores were observed in #5 coal in the study area, but microfractures were well developed, with multiple sets of microfractures exhibiting a vertical intersecting relationship (Figure 3B). Laser confocal quantitative analysis was conducted on seven coal microfractures, and the statistics showed that the shortest length of the microfractures ranged from

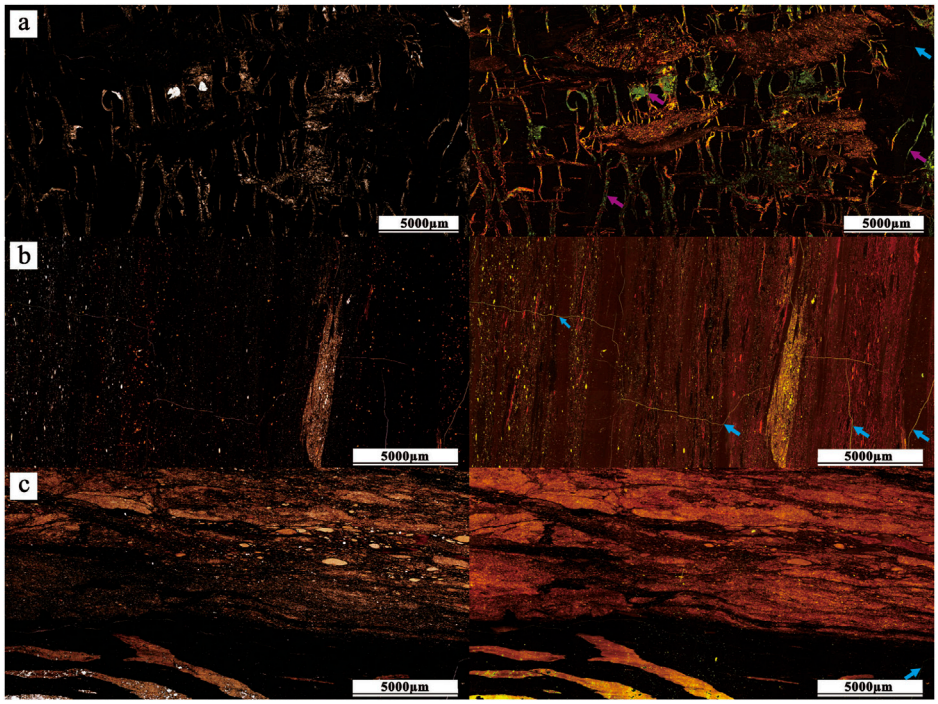

FIGURE 3
Micro macerals and fluorescence micrograph of #5 coal (**(A)**-J26 3030.66 m, **(B)**-T29 2861.07 m, **(C)**-S364 3908.49 m).

20~40 μm, with the majority having lengths between 90~300 μm; early fractures had widths mainly between 50~110 μm, while later fractures had narrower widths, mostly less than 50 μm (Figure 4; Table 1). Significant differences can be quantitatively compared through microscopic scanning. The early microfractures length and width were relatively large simultaneously, which morphology also were uneven, those mainly caused by abnormal high pressure during organic matter hydrocarbon generation. The later microfractures width were relatively small, which morphology were straight and interconnected, that mainly caused by structural stress during deeply burial stage. These microscopic features indicate that Shanxi Formation #5 coal has favorable conditions for cleat generation, which is beneficial for hydraulic fracturing optimization.

The industrial composition of coal mainly consists of four parameters: fixed carbon, ash, volatile matter, and moisture, which are also important indicators for evaluating coal quality (Crosdale et al., 1998). The industrial test data of Shanxi Formation #5 coal indicates significant differences, with fixed carbon content ranging mainly from 45~85%, with a mean of 66.16%; ash content ranging mainly from 10~40%, with a mean of 23.55%; volatile matter ranging mainly from 3~12%, with a mean of 7.51%.By analyzing the ash of the burned #5 coal through X-ray diffraction (XRD), the results show relatively abundant carbonates and quartz, along with small amounts of clay minerals and feldspar, and varying degrees of pyrite. Comparing the trends of fixed carbon and inorganic minerals on a planar scale, it is observed that fixed carbon content decreases from north to south and from east to west, which indicate that the deltaic depositional environments have changed and thus a deterioration in the quality of the coal bed. The quartz increases from north to south, while the carbonate content gradually decreases correspondingly, which trends were associated with the transportation distance, that indicate the sediments originated from the Yinshan uplift in the northern Ordos Basin (Figure 5).

3.3 #5 coal metamorphosis features

During the process of metamorphism, coal rank indicators such as vitrinite reflectance (*Ro*), carbon content (C), and calorific value (Q) are used to determine the degree of coal metamorphism or coalification (Sang et al., 2005). For the #5 coal seam, the vitrinite reflectance *Ro* range is from 0.514% to 2.019%, indicating that the majority of coal seams in the area belong to bituminous coal and are in the middle to high metamorphic stages. The thermal evolution degree gradually increases from north to south (Figure 6), indicating that the overall coal seams are in a stage of significant hydrocarbon generation. There is no obvious correlation between the thermal evolution degree and burial depth in the present state of the #5 coal in the eastern Ordos basin, which is caused by the obvious uplift difference since the Early Cretaceous.

3.4 #5 coal macropores-micropores-fracture system

The adsorption space of coal seam is primarily composed of micropores, accompanied by a small number of small, medium, and

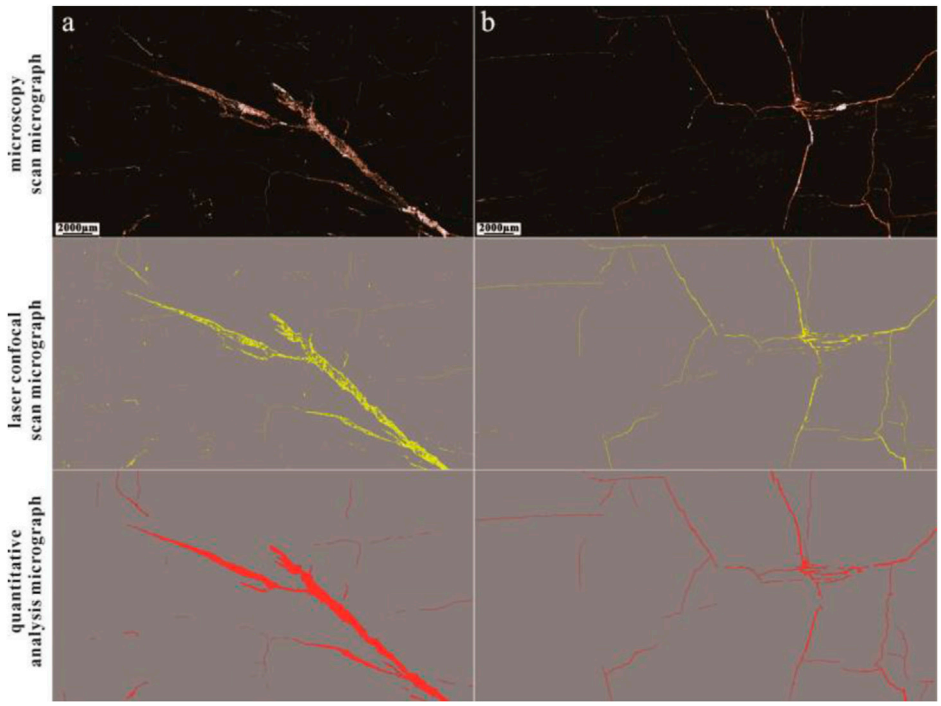

FIGURE 4
Laser confocal scan micrograph and quantitative analysis of #5 coal fractures ((**A**)-J26 3033.45 m, (**B**)-S387 3494.5 m).

TABLE 1 Fracture parametric comparison by laser confocal quantitative analysis.

Well	Depth/m	Frequency	Fracture period	Minimum length/μm	Maximum length/μm	Width average/μm
Y116	2152.25	46	early + later	45.6	220.4	110.7
T49	3214.78	48	early + later	32.3	251.2	74.1
J26	3033.45	33	early + later	23.4	323.4	70.9
S387	3905.62	31	later	35.3	94.7	53.4
Sh102	2663.29	26	later	23.8	77.2	45.6
Q5	2622.93	58	later	27.8	114.3	45.3
Sh95	2441.46	18	later	26.4	50.3	35.8

large pores. They respectively constitute capillary condensation and diffusion regions, areas of slow gas permeation, and intense laminar flow regions (Can et al., 1972; Qin et al., 1995; Ju et al., 2005; Cheng and Hu, 2023). The desorption branch of the isothermal curve of the #5 coal exhibits a stable desorption within a relatively large range of relative pressure (P/P0≈1), with a narrow or absent hysteresis loop, indicating poor development of micropores and mesopores in the #5 coal.

The low-temperature N_2 adsorption indicates that the pore radius is primarily between 10~120 nm, with a mean value of 88.6 nm according to the BET model, and 15.3 nm according to the DFT model (Figure 7A). The low-temperature CO_2 adsorption reveals a pore radius between 1.0~2.0 nm, with a mean value of 1.82 nm according to the BET model (Figure 7B). Both N_2 and CO_2 adsorption results indicate that micro-mesopores smaller than 40 nm are predominant in the #5 coal, with a small number of macropores ranging from 50~100 nm. The adsorption test results suggest that micropores are the primary contributors to specific surface area and pore volume.

The mercury intrusion data indicates that the porosity ranges from 3~8%, with a mean value of 5.32%. The permeability is primarily distributed between (0.05~3) $\mu m^2 \times 10^{-3}$ μm^2, with a median value of 0.37 $\mu m^2 \times 10^{-3}$ μm^2, with few discrete permeability anomalies affected by fractures. The pore-throat radius distribution exhibits a bimodal feature, with half of the median pore-throat radius being less than 0.1 μm, while one-third of the pore-throat radius falls between 0.6~10 μm (Figure 8; Table 2). The small pores smaller than 0.1 μm are mainly organic matter pores and intergranular pores of clay minerals, which quality were controlled by the carbon content and its thermal evolution. Recognized as a microfractures when its pore-throat radius is greater than 1 μm correspondingly,

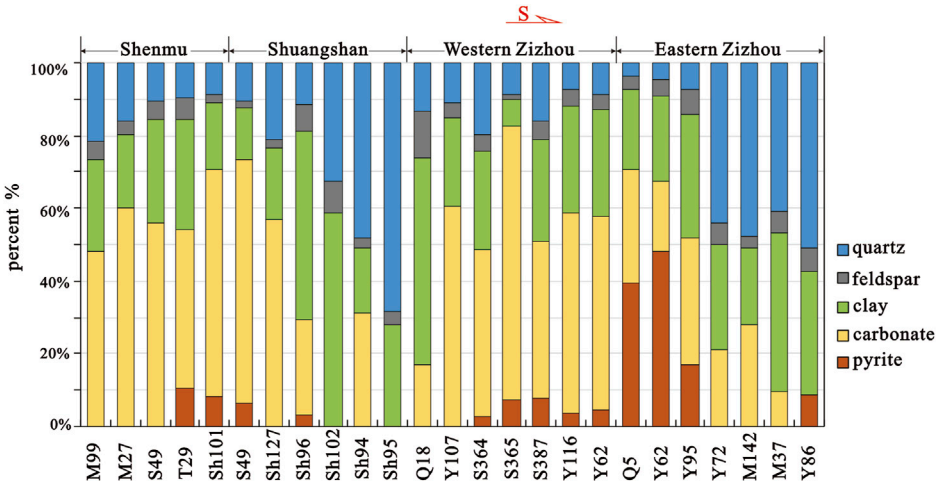

FIGURE 5
Ash distribution trend by XRD of #5 coal.

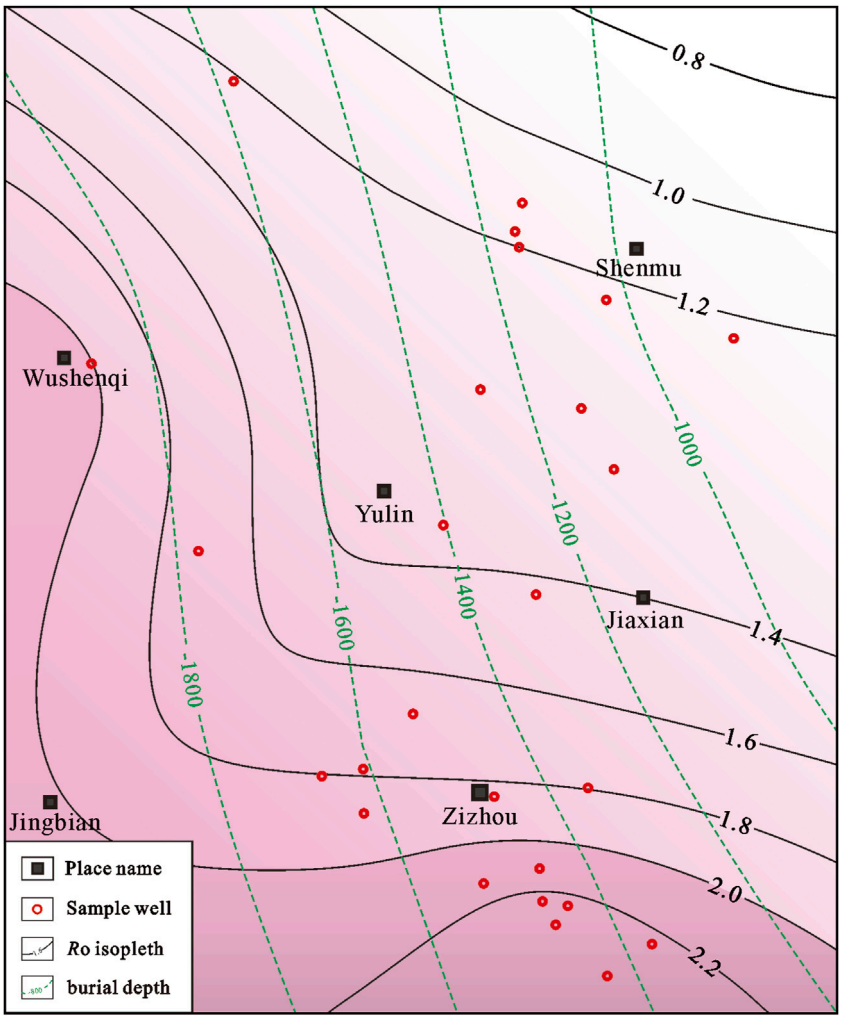

FIGURE 6
Vitrinite reflectance distribution trend of #5 coal.

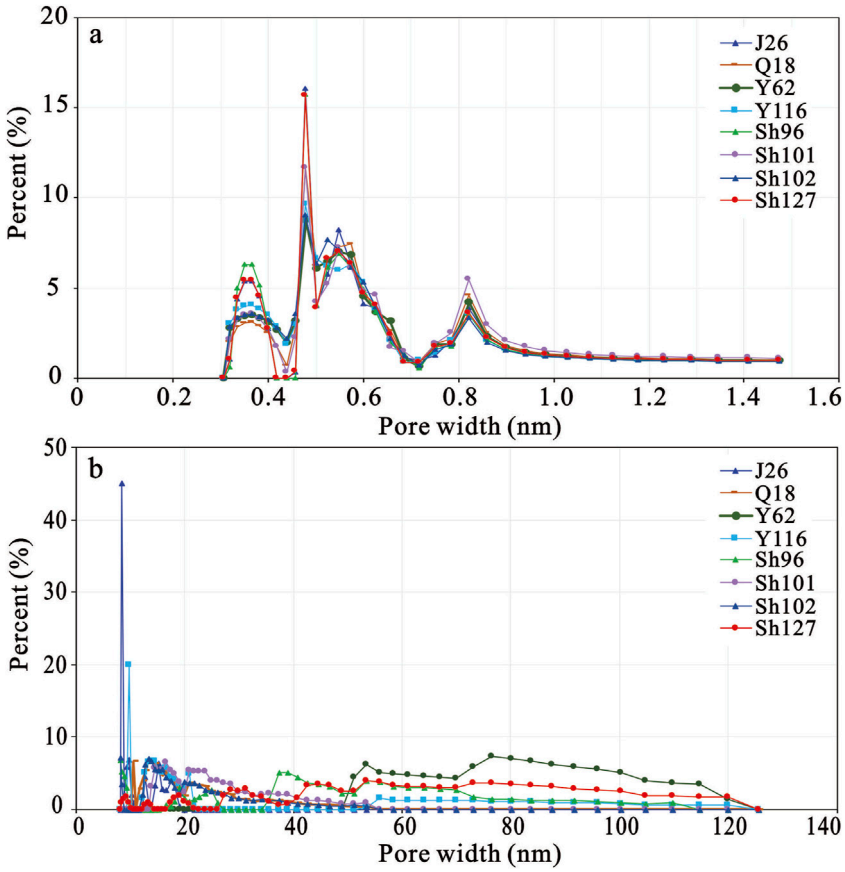

FIGURE 7
The pore radius distribution by low-temperature adsorption ((**A**)-CO_2 adsorption test, (**B**)-N_2 adsorption test).

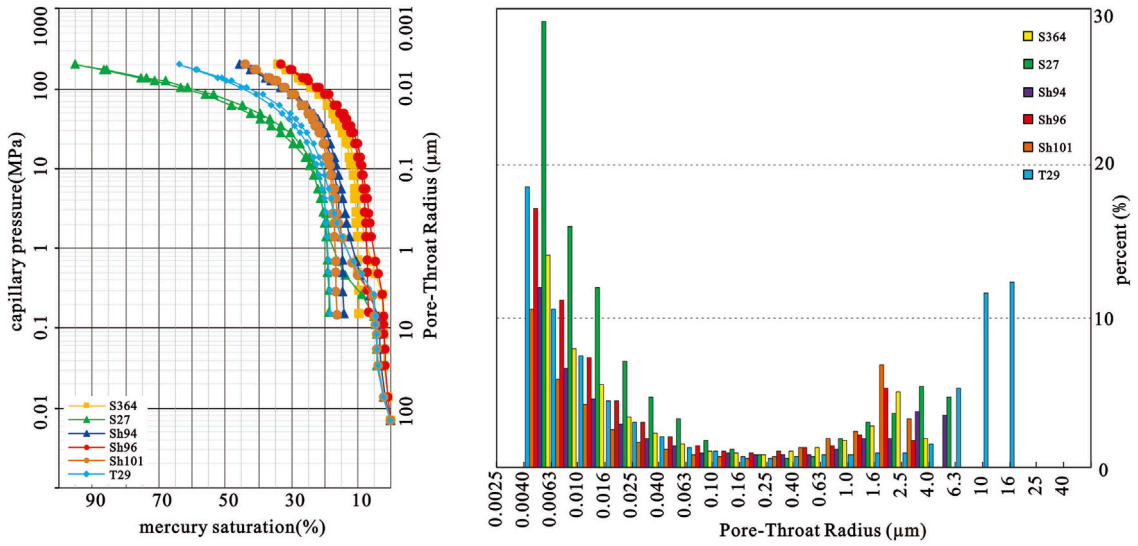

FIGURE 8
Mercury saturation curves and pore-throat radius histogram.

because large pores are difficult to form and preserve in coal bed. The bimodal characteristics of pore throat radius indicating the coexistence of few micrometer-sized fractures and massive nanometer-sized mesopores within the coal, which are significantly different in connectivity and complexity compared with sandstone.

10.3389/fenrg.2024.1406457

TABLE 2 Parametric comparison by high-pressure mercury intrusion of #5 coal.

Well	Depth m	Permeability 10^{-3} μm^2	Porosity %	Pore-throat radius average μm	Pore-throat radius median μm	Mercury saturation max %	Efficiency of mercury withdrawal %	Displacement pressure MPa
T29	2861.07	0.372	2.860	6.305	0.014	83.521	59.171	0.034
S364	3908.49	97.621	6.130	0.452	0.004	50.940	71.565	0.259
Sh94	2094.31	7.843	7.110	0.803	0.001	45.657	68.699	0.138
S27	2060.01	0.181	2.700	0.682	0.010	95.032	80.322	0.138
Sh101	2301.25	3.224	7.420	0.576	0.001	44.078	62.648	0.251
Sh96	2305.07	1.722	6.600	0.382	0.005	60.673	78.919	0.262

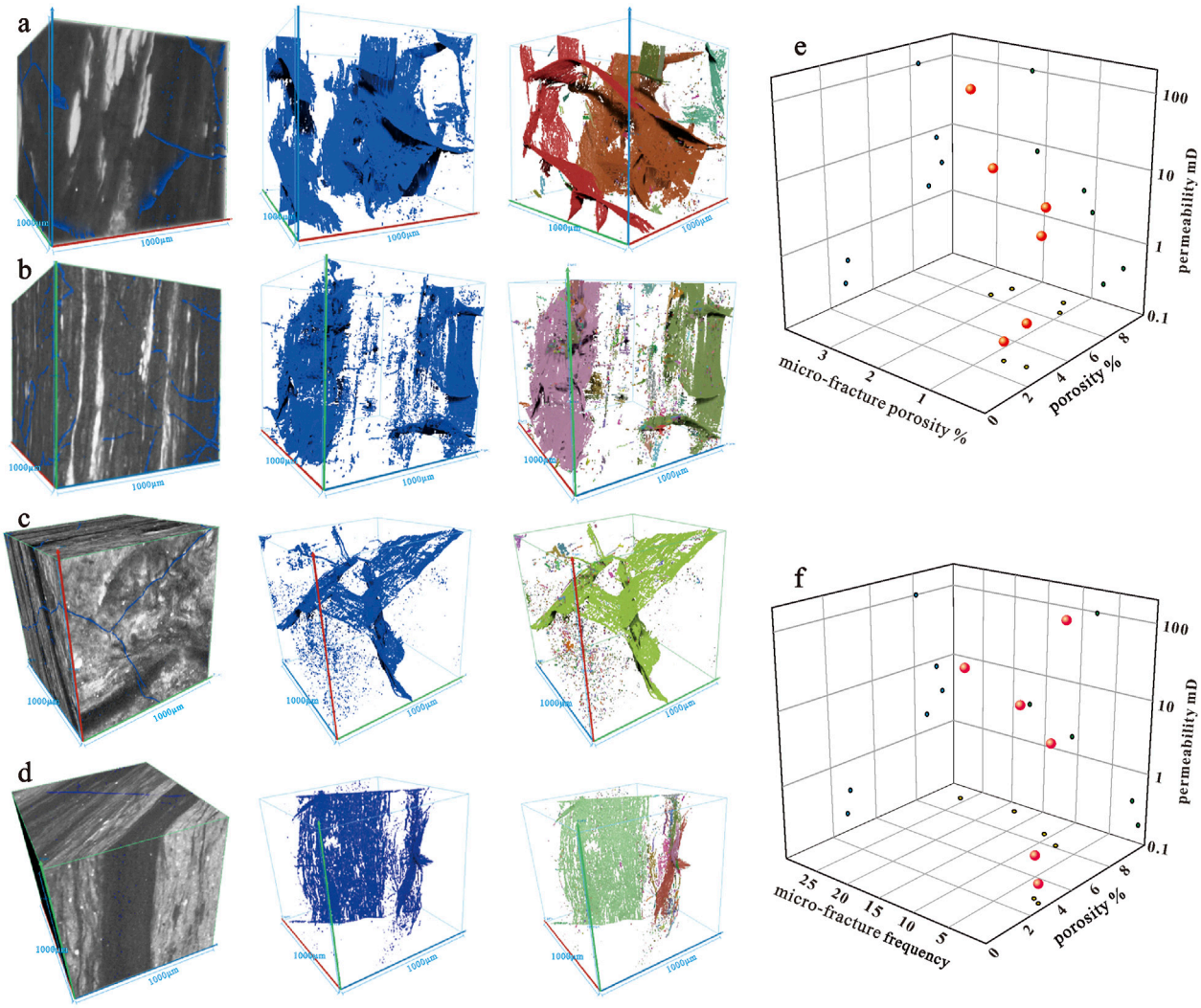

FIGURE 9
3D CT scan micrograph-reconstruction of #5 coal fractures and parametric correlation ((**A**)-S364 3908.49m, (**B**)- Sh101 2301.25m, (**C**)-T49 3214.78m, (**D**)-T29 2861.07m, (**E**)-Positive correlation between porosity, permeability and micro-fracture porosity, (**F**)-Positive correlation between porosity, permeability and micro-fracture frequency).

TABLE 3 Fractures quantitative analysis by 3D CT scan of #5 coal.

Well	Depth/m	Porosity/%	Micropore-fractures volume (mm^3, frequency/Volume present%)				
			>100	10~100	1~10	0.1~1	<0.1
S364	3908.49	1.3	3/90.6	5/6.9	24/1.3	168/0.9	614/0.3
Sh101	2301.25	1.22	2/79.4	16/5.6	145/5.0	1,697/6.7	5,404/3.3
T49	3214.78	0.78	1/89.5	0/0	0/0	20/2.9	775/7.6
T29	2861.07	0.42	0/0	2/71.9	5/12.2	25/5.0	723/10.9

3.5 #5 coal 3D scanning and reconstruction

The advantage of three-dimensional CT scanning method is the fast and non-destructive scanning and imaging of rock samples in all directions and over a wide area. The micro-CT results of Shanxi Formation #5 coal show the significant volume differences between micro-pores and micro-fractures. Among these, fractures with an equivalent diameter greater than 600 μm account for approximately 86% of the total pore and fracture volume, followed by those with equivalent diameters ranging from 10 to 600 μm, which represent approximately 10% of the total pore and fracture volume. Statistical analysis indicates that pores and fractures with an equivalent diameter less than 10 μm constitute 78% of the total number, yet they only contribute to 5.5% of the total pore and fracture volume (Figures 9A–D; Table 3).

The Micro-CT scanning result reveals significant differences in the development of micro-fractures. The number of fractures with a volume less than 0.1 mm^3 is the highest, but their volume ratio is relatively low. Conversely, the number of fractures with a volume greater than 10 mm^3 is the lowest, but their volume ratio is relatively high. Those graphic shows the rock skeleton, all the micro-fractures and micropores are identified as blue, and connected micro-fractures are displayed in the same color about four sample (Figures 9A–D). The correlation is more significant between micro-fracture porosity, micro-fracture frequency and permeability, compared to porosity (Figures 9E, F), which quantitative data indicates that permeability were mainly controlled by micro-fractures rather than micro pores. They exhibit a clear positive correlation: fractures' porosity and permeability, and the number of fractures and permeability, which indicate the fracture system is the main factor of connectivity of the coal bed, which is a supplementary explanation for the bimodal characteristics of pore throat radius system of mercury intrusion data.

Micro-pores can provide a large number of adsorption sites for coalbed methane adsorption and occurrence. Meanwhile, micro-fractures can provide a large amount of storage space and provide space conditions for deep coalbed methane enrichment. Analysis of various test results were adopted to conduct full-scale quantitative characterization of nano-scale pore and micron scale cracks in the pore and fissure structure of coal reservoir, and comprehensively evaluate the pore and fissure structure characteristics of different scales. Multiple test results analysis and evaluation can provide a more scientific basis for judgment in the adsorption capacity and development potential of deep coalbed methane respectively.

The porosity and permeability ranges are essentially similar between #5 and #8 coals, but the monolayer and cumulative thicknesses of #5 coals are significantly thinner. Because of the #8 coals were deposited in the stable swamp sedimentary environments, which is conducive to organic matter enrichment and form stable coal seam structure.

The analysis of coalbed methane logging and hydrocarbon logging, combined with the structural characteristics and heterogeneity of coal reservoirs, demonstrates a positive correlation between coalbed gas measurements and the structure of coal reservoirs. The lithology, pore-fracture structure, and the #5 coal bed thermal evolution determine the heterogeneity of the coal reservoir and the porosity, thereby influencing the gas composition of the coal reservoir.

4 Conclusion

(1) Observations and statistics indicate that approximately three-quarters of the #5 coal consist of primary structural coal, with a trend of increasing cleat density from north to south. There are significant differences in industrial components of #5 coal, with fixed carbon content ranging mainly between 45% and 85%, and ash content mainly between 10% and 40%. XRD testing of the ash content primarily shows carbonates with small amounts of clay. Those cleat density and content in the #5 coal gradually decrease toward the inner basin, caused by transport distance and depositional environment. The microstructures were not similar with the #8 coal, but were more predictable through fluvial depositional environments.

(2) The thermal evolution degree the #5 coal have reached the stage of low-grade anthracite, forming a modern pattern of spreading of coal grades in the eastern Ordos basin, which reduces the differences in micropores-mesopores assemblies due to thermal evolution differences effectively. It is also not necessary to analyze the correlation between present-day burial depth and micropores-mesopores assemblies in #5 coal, which is due to significant uplift differences since the Early Cretaceous.

(3) Multiple test results reveal that the microstructure of the #5 coal is complex. At the micrometer scale, no obvious pores were observed, with the #5 coal mainly comprised of micro-mesopores smaller than 30 nm and a minor amount of macropores ranging from 50~100 nm. Additionally, micro-fractures in the coal were found to be well

developed, which fractures width ranged from 20~110 μm predominantly. The quantify the nanopores and micro-fractures by high-pressure mercury intrusion test and 3D scanning and reconstruction, establish the correlation analysis between the micrometer-scale and nanoscale test results, thereby qualitative analysis the presence of bimodal features of pore throat radius in coal by multiple tests. (4) The differences between pores and micro-fractures are evident and interconnected, with the coal's porosity and connectivity primarily caused by the micro-fracture system, meanwhile micro-fractures also contribute to the pronounced heterogeneity within the #5 coal. Multiple test results analysis and evaluation can provide a more scientific basis for judgment in the adsorption capacity and development potential of deep coalbed methane respectively.

Data availability statement

The raw data supporting the conclusions of this article will be made available by the authors, without undue reservation.

Author contributions

SY: Conceptualization, Data curation, Writing–original draft, Writing–review and editing. ZH: Conceptualization, Data curation, Formal Analysis, Funding acquisition, Writing–original draft, Writing–review and editing. PB: Conceptualization, Data curation, Formal Analysis, Funding acquisition, Writing–review and editing. JX: Conceptualization, Data curation, Formal Analysis, Writing–review and editing. DX: Conceptualization, Data curation, Formal Analysis, Writing–review and editing. ZX: Conceptualization, Data curation, Formal Analysis, Funding acquisition, Investigation, Methodology, Project administration, Software, Writing–review and editing.

Funding

The author(s) declare that financial support was received for the research, authorship, and/or publication of this article. This work was financially supported by CNPC's key applied science and technology project (No.2023ZZ18, Research on deep coal-rock gas accumulation theory and benefit development technology) and Major Science and Technology Project of Changqing Oilfield (No.2023DZZ01, Research on the occurrence mechanism, enrichment law and key technology of effective production improvement of deep coal-rock gas in Ordos Basin). The funders were not involved in the study design, collection, analysis, interpretation of data, the writing of this article, or the decision to submit it for publication.

Conflict of interest

Authors SY, ZH, PB, JX and DX were employed by PetroChina Company Limited Changqing Oilfield Branch.

The remaining author declares that the research was conducted in the absence of any commercial or financial relationships that could be construed as a potential conflict of interest.

Publisher's note

References

Can, H., Nandi, S. P., and Walker, P. L. (1972). Nature of the porosity in American coals. *Fue1* 51 (4), 272–277. doi:10.1016/0016-2361(72)90003-8

Cao, Q., Zhao, J. Z., Fu, J. H., et al. (2013). Gas source conditions of quasi-continuous accumulation of the upper Paleozoic in Ordos basin. *Oil and Gas Geol.* 34 (5), 584–591.

Chalmer, G. R., Bustin, R. M., and Power, I. M. (2012). Characterization of gas shale pore systems by porosimetry, pycnometry, surface area, and field emission scanning electron microscopy/transmission electron microscopy image analyses: examples from the Barnett, Woodford, Haynesville, Marcellus, and Doig units. *AAPG Bull.* 96 (6), 1099–1119. doi:10.1306/10171111052

Chen, Y., Wang, Y., Guo, M., Wu, H., Li, J., Wu, W., et al. (2020). Differential enrichment mechanism of organic matters in the marine-continental transitional shale in northeastern Ordos Basin, China: control of sedimentary environments. *J. Nat. Gas Sci. Eng.* 83, 103625. doi:10.1016/j.jngse.2020.103625

Cheng, Y. P., and Hu, B. (2023). A new pore classification method based on the methane occurrence and migration characteristics in coal. *J. China Coal Soc.* 48 (1), 212–225. doi:10.13225/j.cnki.jccs.Z022.1889

Chou, C. L. (2012). Sulfur in coals: a review of geochemistry and origins. *Int. J. Coal Geol.* 100, 1–13. doi:10.1016/j.coal.2012.05.009

Clarkson, C. R., and Bustin, R. M. (1999). The effect of pore structure and gas pressure upon the transport properties of coal: a laboratory and modeling study 2 Adsorption rate modeling. *Fuel* 78 (11), 1345–1362. doi:10.1016/s0016-2361(99)00056-3

Cnudde, V., and Boone, M. N. (2013). High-resolution x-ray computed tomography in geosciences: a review of the current technology and applications. *Earth-Science Rev.* 123, 1–17. doi:10.1016/j.earscirev.2013.04.003

Crosdale, P. J., Beamish, B. B., and Valix, M. (1998). Coalbed methane sorption related to coal composition. *Int. J. Coal Geol.* 35 (1-4), 147–158. doi:10.1016/s0166-5162(97)00015-3

Dai, S., Ren, D., Tang, Y., Shao, L., and Li, S. (2022). Distribution, isotopic variation and origin of sulfur in coals in the Wuda coalfield, Inner Mongolia, China. *Int. J. Coal Geol.* 51, 237–250. doi:10.1016/s0166-5162(02)00098-8

Hou, S., Wang, X., Wang, X., Yuan, Y., and Pan, S. (2017). Pore structure characterization of low volatile bituminous coals with different particle size and tectonic deformation using low pressure gas adsorption. *Int. J. Coal Geol.* 183, 1–13. doi:10.1016/j.coal.2017.09.013

Hu, B. L., Che, Y., Yang, Q., Liu, D. M., and Huang, W. H. (2003). Analysis on cryogenic nitrogen isothermal adsorption characteristics of coal reservoirs in the Ordos basin. *Coal Geol. and Explor.* 31 (2), 20–23.

Jiang, W. P., Song, X. Z., and Zhong, L. W. (2010). Research on the pore properties of different coal body structure coals and the effects on gas outburst based on the low temperature nitrogen adsorption method. *J. China Coal Soc.* 36 (1), 609–614.

Ju, Y. W., Jiang, B., Hou, Q. L., Wang, G. L., and Fang, A. M. (2005). Structural evolution of nano-scale pores of tectonic coals in Southern North China and its mechanism. *Acta. Geol. Sin.* 79 (2), 269–285.

Levy, J. H., Day, S. J., and Killingley, J. S. (1997). Methane capacities of Bowen Basin coals related to coal properties. *Fuel* 76 (9), 813–819. doi:10.1016/s0016-2361(97)00078-1

Li, W., Yao, H. F., Liu, H. F., Kang, Z. Q., Song, X. X., Feng, Z. Z., et al. (2014). Advanced characterization of three-dimensional pores in coals with different coal-body structure by micro-CT. *J. China Coal Soc.* 39 (6), 1127–1132. doi:10.13225/j.cnki.jccs.2013.0920

Li, X. C., Chen, D. F., Kang, Y. L., and Meng, X. J. (2016). Characterization of pores and fractures of coal based on CT scan. *Coal Geol. Explor.* 44 (5), 58–62.

Li, Y., Meng, S. Z., Wu, P., and Niu, X. L. (2017). Accumulation mechanisms and classification of CBM reservoir types: a case study from the eastern margin of the Ordos Basin. *Nat. Gas. Ind.* 37 (8), 22–30.

Li, Y., Yang, J., Pan, Z., Meng, S., Wang, K., and Niu, X. (2019). Unconventional natural gas accumulations in stacked deposits: a discussion of Upper Paleozoic coal-bearing strata in the east margin of the Ordos Basin, China. *Acta Geol. Sin. Engl. Ed.* 93 (1), 111–129. doi:10.1111/1755-6724.13767

Liu, X. S., Zhou, L. F., and Hou, Y. D. (2007). Study of gas charging in the upper Paleozoic of Ordos basin using fluid inclusion. *Acta Pet. Sin.* 28 (6), 37–42.

Nie, B., Liu, X., Yang, L., Meng, J., and Li, X. (2015). Pore structure characterization of different rank coals using gas adsorption and scanning electron microscopy. *Fuel* 158, 908–917. doi:10.1016/j.fuel.2015.06.050

Qin, Y., and Shen, J. (2016). On the fundamental issues of deep coalbed methane geology. *Acta Pet. Sin.* 37 (1), 125–136.

Qin, Y., Xu, Z. W., and Zhang, J. (1995). Natural classification of the high-rank coal pore structure and its application. *J. China Coal Soc.* 20 (3), 266–271.

Sang, S. X., Zhu, Y. M., Zhang, S. Y., Zhang, J., and Tang, J. X. (2005). Solid-gas interaction mechanism of coal-adsorbed gas(I)-Coal pore structure and solid-gas interaction. *Nat. Cas. Ind.* 25 (1), 13–15.

Shan, S. M., Crawshaw, J. P., and Boek, L. S. (2014). Preparation of microporous rock samples for confocal laser scanning microscopy. *Pet. Geosci.* 20 (4), 369–374. doi:10.1144/petgeo2014-021

Song, B. Y., Song, D. Y., Ii, C. H., and Yuan, L. (2017). Influence of magmatic intrusion on the coal basis of mercury intrusion porosimeter. *Coal Geol. and Explor.* 15 (3), 7–12.

Stach, E., Mackowsky, M., Teichmüller, M., Taylor, G. H., Chandra, D., Teichmüller, R., et al. (1990). *Stach's textbook of coal petrology[M]. Translated by Yang Qi.* Beijing: Coal industry publishing house.

Tissot, B. P., and Welte, D. H. (1984). *Petroleum Formation and occurrence*. New York: Springer, 98–110.

Torsvik, T. H., and Cocks, L. R. M. (2004). Earth geography from 400 to 250 Ma: a palaeomagnetic, faunal and facies review. *Geol. Soc.* 161, 555–572. doi:10.1144/0016-764903-098

Yang, H., Fu, J. H., Liu, X. S., and Meng, P. (2012). Accumulation conditions and exploration and development of tight gas in the upper Paleozoic of the Ordos basin. *Petroleum Explor. Dev.* 39 (3), 315–324. doi:10.1016/s1876-3804(12)60047-0

Yao, Y. B., Liu, D. M., Cai, Y. D., and Li, J. Q. (2010). Advanced characterization of pores and fractures in coals by nuclear magnetic resonance and X-ray computed tomography. *Sci. China Earth Sci.* 53 (6), 854–862. doi:10.1007/s11430-010-0057-4

Zhao, J. Z., Cao, Q., Bai, Y. B., Er, C., Li, J., Wu, W., et al. (2017). Petroleum accumulation: from the continuous to discontinuous. *Petroleum Res.* 02, 131–145. doi:10.1016/j.ptlrs.2017.02.001

Zhao, J. Z., Fu, J. H., Yao, J. L., Liu, X. S., and Wang, H. E. (2013). Quasi-continuous accumulation model of large tight sandstone gas field in Ordos's basin. *Acta Pet. Sin.* 33 (S1), 37–52.

Zhao, W. B., Liu, H. L., Wang, H. C., et al. (2023). Research on the controlling effect of coal facies on pore structure - deeply buried coal seam 8 # in yulin area, Ordos Basin for example[J/OL]. *Coal Sci. Technol.*, doi:10.12438/cst.2023-1112